

String-breaking of the triply heavy baryon at finite temperature and chemical potential

Jia-Jie Jiang¹, Xun Chen^{1,2,*}, Jiajia Qin^{1,†} and Miguel Angel Martin Contreras^{1,‡}

¹*School of Nuclear Science and Technology, University of South China, Hengyang 421001, China*

²*Key Laboratory of Quark and Lepton Physics (MOE), Central China Normal University, Wuhan 430079, China*

 (Received 10 October 2023; accepted 9 November 2023; published 4 December 2023)

In this work, we use gauge/gravity duality to study potential energy and string breaking of triply heavy baryons at finite temperature and chemical potential. Two different possible configurations of triply heavy baryon are considered. The effect of temperature and chemical potential on string-breaking distance is investigated. With increasing temperature/chemical potential, the string-breaking distance decreases and then increases in symmetric collinear geometry while steadily increasing in equilateral triangle geometry. Our study provides insights into triply heavy baryon configuration and string-breaking behavior.

DOI: [10.1103/PhysRevD.108.126002](https://doi.org/10.1103/PhysRevD.108.126002)

I. INTRODUCTION

In the SU(3) quenched lattice QCD, the three-quark potential is found to be well-reproduced by

$$V_{3Q}(\mathbf{r}_1, \mathbf{r}_2, \mathbf{r}_3) = \sigma_{3Q} L_{\min} - \sum_{i < j} \frac{A_{3Q}}{|\mathbf{r}_i - \mathbf{r}_j|} + C_{3Q}. \quad (1)$$

Here \mathbf{r}_1 , \mathbf{r}_2 , and \mathbf{r}_3 are the positions of the three quarks, and L_{\min} is the minimum flux-tube length connecting the three quarks. The strength of quark confinement is controlled by the string tension σ_{3Q} of the flux tube. In the hadron model, baryons are composed of three quarks, which are linked together by a Y-shaped configuration [1–5].

AdS/CFT is a useful means to deal with QCD problems. The results can provide important information about the QCD properties of the nonperturbative energy region [6–8]. Oleg Andreev has proposed effective multi-quark potential models from holography at vanishing temperature and chemical potential [9–15], we recently studied the triply heavy baryon at finite temperature and chemical potential from holography [16].

The fragmentation methods of the three-quark QQQ are as follows [13]:

$$\begin{aligned} \nearrow QQQ + Q\bar{q} \\ QQQ &\rightarrow Qq + 2Q\bar{q}\bar{q} \\ \searrow qqq + 3Q\bar{q}. \end{aligned} \quad (2)$$

According to lattice calculations in SU(3) gauge theory, the potential energy between three heavy quarks increases linearly with distance as they are pulled apart [17]. The potential energy becomes saturated when the distance between quarks reaches a certain length, causing the string connecting the three quarks to break. As a result, new quark states and quark-antiquark pairs are generated [18]. In string models of hadrons, such a phenomenon is interpreted as string-breaking [1–3]. This particular distance sets a characteristic scale called the string-breaking distance [19,20]. This scale is obtained from the following formula:

$$E_{Q\bar{Q}}(\mathcal{L}_{Q\bar{Q}}) = 2E_{Qq}. \quad (3)$$

We apply the same method to determine the string-breaking length in the three-quark state. Three quarks exhibit different potential energies at the same chord distance depending on finite temperatures and chemical potentials. If we assume that hadrons are noninteracting, the total energy is the sum of the energies of individual hadrons [13]. When we observe that quark models of different states possess equal energy and their linear potentials are identical, it is inferred that they have the potential to undergo string breaking.

The study of the triple heavy quark potential and its string breaking has been one of the key issues in quantum chromodynamics [21]. QCD string fracture research has a long history [22–26]. The lattice calculations and AdS/CFT approaches have been studied accordingly [27–29].

*chenxunhep@qq.com

†jiijiaqin@usc.edu.cn

‡miguelangel.martin@usc.edu.cn

Published by the American Physical Society under the terms of the Creative Commons Attribution 4.0 International license. Further distribution of this work must maintain attribution to the author(s) and the published article's title, journal citation, and DOI. Funded by SCOAP³.

The existing literature primarily focuses on the stability and decay mode of triple-heavy quarks under zero-temperature chemical potential conditions [18,30,31], while the effect of the temperature chemical potential is less considered [16,32]. In order to gain a deeper understanding of the configuration behavior of triple-heavy quarks, we have systematically investigated, for the first time, the effect of the temperature chemical potential on the string-breaking distance of triple heavy quarks using holographic theory. Studying the string-breaking process helps to reveal the breaking mechanism of triple-heavy quarks.

The article is organized as follows. In Sec. II, we will provide the potential energy calculation formulas for QQQ , QQq , $Qq\bar{q}$, Qqq , and qqq , respectively. In Sec. III, we will draw potential energy diagrams for various hadrons and calculate the string-breaking results. In Sec. IV, we will summarize the results of our work.

II. MODEL

We choose the deformed anti-de Sitter–Reissner–Nordström (AdS-RN) metric. It is not a self-consistent solution to the Einstein equation. However, it gains some insights into problems without predictions from phenomenology and lattice QCD. The background is of the form [9,33]

$$dS^2 = e^{sr^2} \frac{R^2}{r^2} [f(r)dt^2 + d\vec{x}^2 + f^{-1}(r)dr^2],$$

$$f(r) = 1 - \left(\frac{1}{r_h^4} + q^2 r_h^2 \right) r^4 + q^2 r^6. \quad (4)$$

Here, q is the black hole charge, and r_h is the position of the black hole horizon. The Hawking temperature of the black hole is defined as

$$T = \frac{1}{4\pi} \left. \frac{df}{dr} \right|_{r=r_h} = \frac{1}{\pi r_h} \left(1 - \frac{1}{2} Q^2 \right), \quad (5)$$

where $Q = qr_h^3$ and $0 \leq Q \leq \sqrt{2}$ [34]. It is observed that, on dimensional grounds, the low- r behavior of the bulk gauge field $A_0(r)$ is [35]

$$A_0(r) = \mu - \eta r^2, \quad (6)$$

where $\eta = \kappa q$ with κ being a dimensionless parameter. Together with the condition that A_0 vanishes at the horizon $A_0(r_h) = 0$ and $A_0(0) = \mu$, we can determine a relation between μ and the black hole charge q ,

$$\mu = q\kappa r_h^2 = \kappa \frac{Q}{r_h}. \quad (7)$$

We fix the parameter κ to 1 in this paper. The AdS/CFT dictionary defines μ as the baryon number chemical potential. Thus, we can get

$$f(r) = 1 - \left(\frac{1}{r_h^4} + \frac{\mu^2}{r_h^2} \right) r^4 + \frac{\mu^2}{r_h^4} r^6,$$

$$T = \frac{1}{\pi r_h} \left(1 - \frac{1}{2} \mu^2 r_h^2 \right),$$

$$A_0(r) = \mu - \mu \frac{r^2}{r_h^2}. \quad (8)$$

The first is the fundamental string governed by the Nambu-Goto action. By using the static gauge $t = \tau$, $\sigma = x$, the Nambu-Goto action of the U-shape string is [36]

$$S_{\text{NG}} = \frac{1}{2\pi\alpha'} \int d\tau d\sigma \sqrt{\det g_{\alpha\beta}}, \quad (9)$$

with

$$g_{\alpha\beta} = G_{\mu\nu} \frac{\partial x^\mu}{\partial \sigma^\alpha} \frac{\partial x^\nu}{\partial \sigma^\beta}, \quad (10)$$

where X^μ and $G_{\mu\nu}$ are the target space coordinates and the metric, respectively, and σ^α with $\sigma = 0, 1$ parametrize the world sheet.

The baryon vertex is given by [37,38]

$$S_{\text{vert}} = \tau_v \int dt \frac{e^{-2sr^2}}{r} \sqrt{f(r)}, \quad (11)$$

where τ_v is a dimensionless parameter defined by $\tau_v = \mathcal{T}_5 R \text{vol}(\mathbf{X})$, and $\text{vol}(\mathbf{X})$ is a volume of \mathbf{X} . We consider the light quarks at string endpoints as tachyon fields. Thus, we add to the world sheet action $S_q = \int d\tau eT$, which is the usual sigma-model action for strings propagating in a tachyon background [38]. The action written in the static gauge is

$$S_q = m \int dt \frac{e^{sr^2}}{r} \sqrt{f(r)}, \quad (12)$$

where $m = RT_0$. We immediately recognize it as the action of a point particle of mass T_0 at rest [39]. In the presence of a background gauge field, the string endpoints with attached quarks couple to it. So the world sheet action includes boundary terms given by

$$S_A = \mp \frac{1}{3} \int dt A_0, \quad (13)$$

where the minus-plus sign corresponds to a quark and an antiquark, respectively. We will choose model parameters as follows: $g = \frac{R^2}{2\pi\alpha'}$, $k = \frac{\tau_v}{3g}$, and $n = \frac{m}{g}$.

A. QQQ model

The total action of three-quark potential is the sum of the three Nambu-Goto actions plus the vertex action and the boundary action terms

$$S = \sum_{i=1}^3 S_{\text{NG}}^{(i)} + S_{\text{vert}} + 3S_A|_{r=0}. \quad (14)$$

Thus, the action can now be written as

$$S = \frac{3g}{T} \int dx \frac{e^{sr^2}}{r^2} \sqrt{f(r) + (\partial_x r)^2} + \frac{3kg}{T} \frac{e^{-2sr_v^2}}{r_v} \sqrt{f(r_v)} - \frac{A_0(0)}{T}, \quad (15)$$

with $T = \int_0^T dt$. The Lagrangian is written as

$$\mathcal{L} = \frac{e^{sr^2}}{r^2} \sqrt{f(r) + (\partial_x r)^2}, \quad (16)$$

altogether, with the constraint

$$\mathcal{L} - r' \frac{\partial \mathcal{L}}{\partial r'} = \frac{\frac{e^{sr^2}}{r^2} f(r)}{\sqrt{f(r) + (\partial_x r)^2}} = \text{constant}. \quad (17)$$

At the points r_0 and r_v , we have

$$\begin{aligned} \frac{\frac{e^{sr^2}}{r^2} f(r)}{\sqrt{f(r) + (\partial_x r)^2}} &= \frac{e^{sr_0^2}}{r_0^2} \sqrt{f(r_0)}, \\ \frac{\frac{e^{sr_v^2}}{r_v^2} f(r_v)}{\sqrt{f(r_v) + \tan^2 \alpha}} &= \frac{e^{sr_0^2}}{r_0^2} \sqrt{f(r_0)}. \end{aligned} \quad (18)$$

The above equations can determine the relation between r_0 , r_v , and α . We can also get

$$\partial_r x = \sqrt{\frac{\frac{e^{2sr_0^2}}{r_0^4} f^2(r_0)}{\frac{e^{2sr^2}}{r^4} f^2(r) f(r_0) - \frac{e^{2sr_0^2}}{r_0^4} f^2(r_0) f(r)}}, \quad (19)$$

and

$$\frac{e^{sr_v^2}}{r_v^2} f(r_v) - \frac{e^{sr_0^2}}{r_0^2} \sqrt{f(r_0)} \sqrt{f(r_v) + \tan^2 \alpha} = 0. \quad (20)$$

At this step, we must find the relationship between r_v and α . We can obtain the result through the equilibrium condition at the baryon vertex. This differs between the three-quark (A) and three-quark (B) models. The force balance equation at the point $r = r_v$ is

$$\mathbf{e}_1 + \mathbf{e}_2 + \mathbf{e}_3 + \mathbf{f}_v = \mathbf{0}, \quad (21)$$

where \mathbf{e}_i is the string tension and \mathbf{f}_v is the gravitational force acting on the vertex. The presence of this force is the main difference between string models in flat spaces and those in curved spaces. In this model, \mathbf{f}_v only has one nonzero component in the r -direction. A formula for this component can be derived from the action $E_{\text{vert}} = T \cdot S_{\text{vert}}$. Explicitly, $f'_v = -\delta E_{\text{vert}} / \delta r$ and r is the coordinate of the vertex. The possible configurations of the triply heavy baryon are shown in Fig. 1.

1. QQQ(A) equilateral triangle geometry

In the three-quark(A), each force is given by

$$\begin{aligned} \mathbf{f}_v &= \left(0, 0, -3gk \frac{e^{-2sr_v^2}}{r_v} \sqrt{f(r_v)} \right), \\ \mathbf{e}_1 &= -g \frac{e^{sr_v^2}}{r_v^2} \left(\cos \beta \frac{f(r_v)}{\sqrt{f(r_v) + \tan^2 \alpha}}, \sin \beta \frac{f(r_v)}{\sqrt{f(r_v) + \tan^2 \alpha}}, -\frac{1}{\sqrt{1 + f(r_v) \cot^2 \alpha}} \right), \\ \mathbf{e}_2 &= -g \frac{e^{sr_v^2}}{r_v^2} \left(-\cos \beta \frac{f(r_v)}{\sqrt{f(r_v) + \tan^2 \alpha}}, \sin \beta \frac{f(r_v)}{\sqrt{f(r_v) + \tan^2 \alpha}}, -\frac{1}{\sqrt{1 + f(r_v) \cot^2 \alpha}} \right), \\ \mathbf{e}_3 &= -g \frac{e^{sr_v^2}}{r_v^2} \left(0, -\frac{f(r_v)}{\sqrt{f(r_v) + \tan^2 \alpha}}, -\frac{1}{\sqrt{1 + f(r_v) \cot^2 \alpha}} \right). \end{aligned} \quad (22)$$

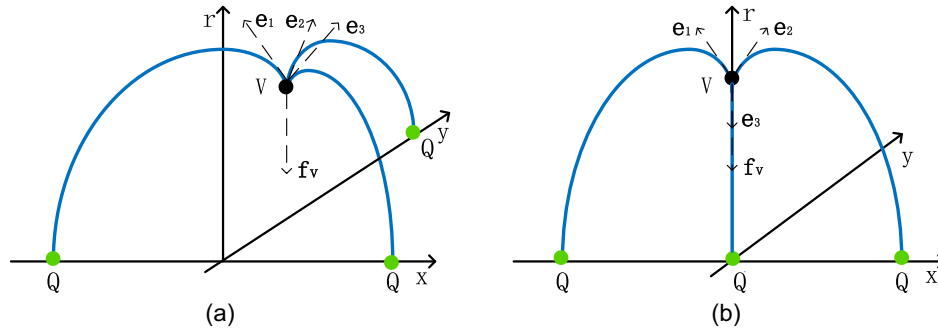


FIG. 1. (a) The heavy quarks are at the vertices of the equilateral triangle for QQQ. (b) Symmetric collinear geometry for QQQ.

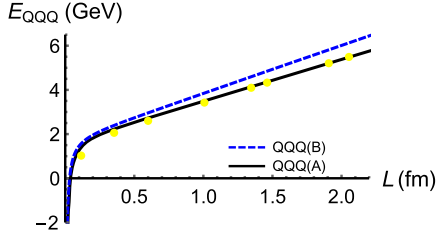


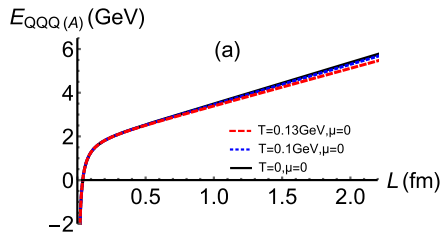
FIG. 2. The potential energy for three-heavy quarks (heavy baryons) as a function of the separation distance at vanishing temperature. The dots are the results of lattice QCD [40]. Here $s = 0.450$ GeV [41], $g = 0.176$ [20], $k = -0.102$ [42], and $c = 0.623$ GeV [13].

Regarding the symmetry in x and y , we only need to consider the force balance in the r direction. The force-balance equation leads to

$$\frac{e^{sr_v^2}}{r_v^2} \frac{1}{\sqrt{1 + f(r_v)\cot^2\alpha}} - k\partial_{r_v} \frac{e^{-2sr_v^2}}{r_v} \sqrt{f(r_v)} = 0. \quad (23)$$

Therefore, L and E can be calculated as

$$\begin{aligned} L &= \sqrt{3} \left(\int_0^{r_0} \partial_r x dr + \int_{r_v}^{r_0} \partial_r x dr \right) \\ &= \sqrt{3} \int_0^{r_0} \sqrt{\frac{\frac{e^{2sr_0^2}}{r_0^4} f^2(r_0)}{\frac{e^{2sr^2}}{r^4} f^2(r) f(r_0) - \frac{e^{2sr_0^2}}{r_0^4} f^2(r_0) f(r)}}} dr \\ &\quad + \sqrt{3} \int_{r_v}^{r_0} \sqrt{\frac{\frac{e^{2sr_0^2}}{r_0^4} f^2(r_0)}{\frac{e^{2sr^2}}{r^4} f^2(r) f(r_0) - \frac{e^{2sr_0^2}}{r_0^4} f^2(r_0) f(r)}}} dr, \quad (24) \\ E &= 3g \left(\int_0^{r_0} \frac{e^{sr^2}}{r^2} \sqrt{1 + f(r)(\partial_r x)^2} - \frac{1}{r^2} dr \right. \\ &\quad \left. + \int_{r_v}^{r_0} \frac{e^{sr^2}}{r^2} \sqrt{1 + f(r)(\partial_r x)^2} dr \right) \\ &\quad - \frac{3g}{r_0} + 3gk \frac{e^{-2sr_v^2}}{r_v} \sqrt{f(r_v)} + 3c - \mu. \quad (25) \end{aligned}$$



The potential energy of the three-quark ground state is shown in Fig. 2 and the potential energy of model A at different temperatures and chemical potentials is shown in Fig. 3.

2. QQQ(B) symmetric collinear geometry

In the three-quark(B), each force is given by

$$\begin{aligned} \mathbf{f}_v &= \left(0, -3gk\partial_{r_v} \frac{e^{-2sr_v^2}}{r_v} \sqrt{f(r_v)} \right), \\ \mathbf{e}_1 &= -g \frac{e^{sr_v^2}}{r_v^2} \left(\frac{f(r_v)}{\sqrt{f(r_v) + \tan^2\alpha}}, -\frac{1}{\sqrt{1 + f(r_v)\cot^2\alpha}} \right), \\ \mathbf{e}_2 &= -g \frac{e^{sr_v^2}}{r_v^2} \left(-\frac{f(r_v)}{\sqrt{f(r_v) + \tan^2\alpha}}, -\frac{1}{\sqrt{1 + f(r_v)\cot^2\alpha}} \right), \\ \mathbf{e}_3 &= -g \frac{e^{sr_v^2}}{r_v^2} (0, 1), \quad (26) \end{aligned}$$

with the force balance equation

$$-2 \frac{e^{sr_v^2}}{r_v^2} \frac{1}{\sqrt{1 + f(r_v)\cot^2\alpha}} + \frac{e^{sr_v^2}}{r_v^2} + 3k\partial_{r_v} \frac{e^{-2sr_v^2}}{r_v} \sqrt{f(r_v)} = 0. \quad (27)$$

Thus, we can similarly obtain interquark distance

$$\begin{aligned} L &= \int_0^{r_0} \partial_r x dr + \int_{r_v}^{r_0} \partial_r x dr \\ &= \int_0^{r_0} \sqrt{\frac{\frac{e^{2sr_0^2}}{r_0^4} f^2(r_0)}{\frac{e^{2sr^2}}{r^4} f^2(r) f(r_0) - \frac{e^{2sr_0^2}}{r_0^4} f^2(r_0) f(r)}}} dr \\ &\quad + \int_{r_v}^{r_0} \sqrt{\frac{\frac{e^{2sr_0^2}}{r_0^4} f^2(r_0)}{\frac{e^{2sr^2}}{r^4} f^2(r) f(r_0) - \frac{e^{2sr_0^2}}{r_0^4} f^2(r_0) f(r)}}} dr, \quad (28) \end{aligned}$$

and the potential energy as in Model A.

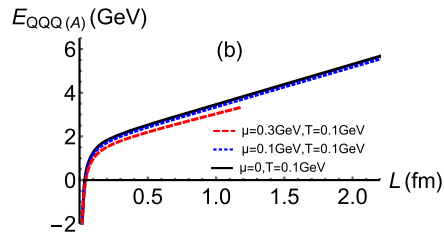


FIG. 3. Model A: Panel (a) shows the potential energy diagram for different temperatures at a zero chemical potential. Panel (b) presents the potential energy diagram for different chemical potentials at a temperature of $T = 0.1$ GeV.

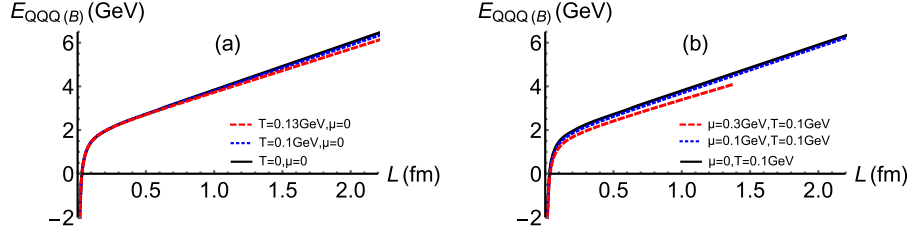


FIG. 4. Model B: Panel (a) represents the potential energy diagram for different temperatures at zero chemical potential. Panel (b) illustrates the potential energy diagram for different chemical potentials at a temperature of $T = 0.1$ GeV.

$$\begin{aligned}
 E = & 2g \left(\int_0^{r_0} \frac{e^{sr^2}}{r^2} \sqrt{1 + f(r)(\partial_r x)^2} - \frac{1}{r^2} dr \right. \\
 & \left. + \int_{r_v}^{r_0} \frac{e^{sr^2}}{r^2} \sqrt{1 + f(r)(\partial_r x)^2} dr \right) \\
 & - \frac{2g}{r_0} + g \int_0^{r_v} \frac{e^{sr^2}}{r^2} - \frac{1}{r^2} dr - \frac{g}{r_v} \\
 & + 3gk \frac{e^{-2sr_v^2}}{r_v} \sqrt{f(r_v)} + 3c - \mu. \quad (29)
 \end{aligned}$$

The potential energy diagram of Model B with different temperatures and chemical potentials is shown in Fig. 4.

B. QQq model

In this section, we will focus on discussing the cases of QQq. The configuration of QQq will vary with the distance between the quarks, and for our model, QQq is divided into three cases. The different configurations of QQq are depicted in Fig. 5.

1. QQq small

In this case, the total effect can be expressed as

$$S = \sum_{i=1}^3 S_{\text{NG}}^{(i)} + S_{\text{vert}} + S_q + 2S_A|_{r=0} + S_A|_{r=r_q}. \quad (30)$$

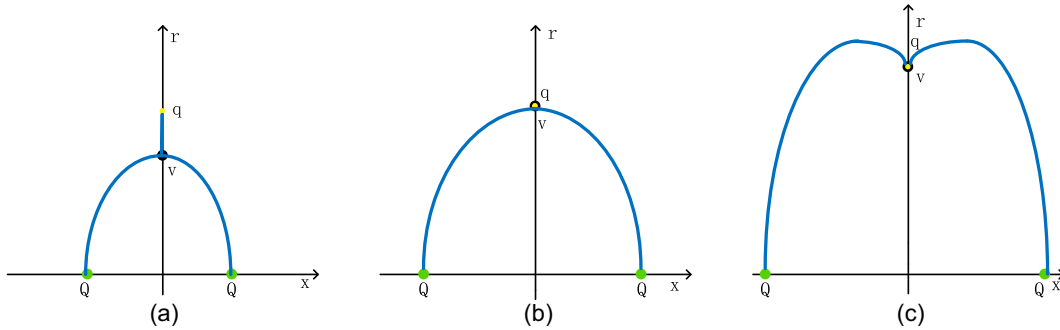


FIG. 5. According to different string distances, we classify QQq into three distinct states. In the subsequent part, we will discuss the calculation methods for the potential energy of each state. For our model calculations, we adopt the following parameters: $s = 0.450$ GeV, $g = 0.176$, $n = 3.057$ [20], $k = -\frac{1}{4}e^{\frac{1}{2}}$ [20], and $c = 0.623$ GeV. Here, we use different values for the k -value because we are using a specific model [13].

The full action can be written as

$$\begin{aligned}
 S = & \frac{2g}{T} \int dx \frac{e^{sr^2}}{r^2} \sqrt{f(r) + (\partial_x r)^2} + \frac{3kg}{T} \frac{e^{-2sr_v^2}}{r_v} \sqrt{f(r_v)} \\
 & + \frac{ng}{T} \frac{e^{\frac{1}{2}sr_v^2}}{r_v} \sqrt{f(r_v)} - \frac{2A_0(0)}{3} \frac{1}{T} - \frac{1A_0(r_q)}{3} \frac{1}{T}. \quad (31)
 \end{aligned}$$

Thus, we have

$$\mathcal{L} = w(r) \sqrt{f(r) + (\partial_x r)^2}, \quad w(r) = \frac{e^{sr^2}}{r^2} \quad (32)$$

and

$$\mathcal{L} - r' \frac{\partial \mathcal{L}}{\partial r'} = \frac{w(r)f(r)}{\sqrt{f(r) + (\partial_x r)^2}} = \text{constant}. \quad (33)$$

Using the conservation of energy, we have

$$\frac{w(r)f(r)}{\sqrt{f(r) + (\partial_x r)^2}} = \frac{w(r_v)f(r_v)}{\sqrt{f(r_v) + \tan^2 \alpha}}$$

at the U -shape string maximum point r_0 . Thus, we get

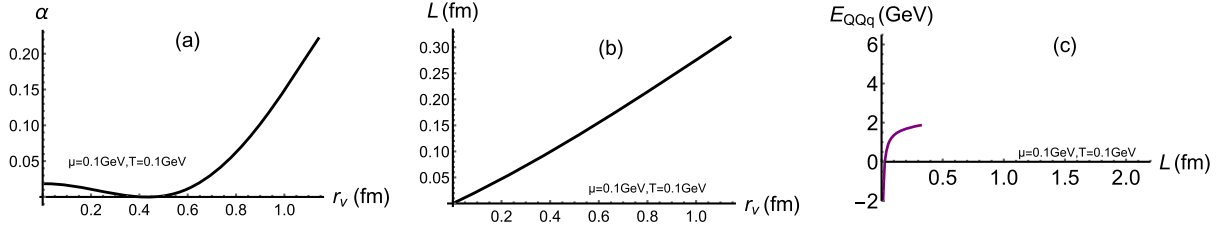


FIG. 6. (a) α as a function of r_v . (b) Separation distance L as a function of r_v . (c) The energy E as a function of L at $\mu = 0.1$ GeV, $T = 0.1$ GeV.

$$\partial_r x = \sqrt{\frac{\omega(r_v)^2 f(r_v)^2}{(f(r_v) + \tan^2 \alpha) \omega(r)^2 f(r)^2 - f(r) w(r_v)^2 f(r_v)^2}}. \quad (34)$$

For the force equilibrium in the model,

$$\mathbf{f}_v = \left(0, -3gk \partial_{r_v} \left(\frac{e^{-2sr_v^2}}{r_v} \sqrt{f(r_v)} \right) \right),$$

and string tensions are

$$\mathbf{e}_1 = gw(r_v) \left(-\frac{f(r_v)}{\sqrt{\tan^2 \alpha + f(r_v)}}, -\frac{1}{\sqrt{f(r_v) \cot^2 \alpha + 1}} \right),$$

$$\mathbf{e}_2 = gw(r_v) \left(\frac{f(r_v)}{\sqrt{\tan^2 \alpha + f(r_v)}}, -\frac{1}{\sqrt{f(r_v) \cot^2 \alpha + 1}} \right),$$

$$\mathbf{e}_3 = gw(r_v)(0, 1).$$

Therefore, after imposing force equilibrium at the vertex

$$\mathbf{e}_1 + \mathbf{e}_2 + \mathbf{e}_3 + \mathbf{f}_v = 0 \quad (35)$$

we obtain the force balance equation given by

$$2g \frac{e^{sr_v^2}}{r_v^2} \frac{1}{\sqrt{1 + f(r_v) \cot^2 \alpha}} - g \frac{e^{sr_v^2}}{r_v^2} + 3gk \left(\frac{e^{-2sr_v^2}}{r_v} \sqrt{f(r_v)} \right)' = 0. \quad (36)$$

As the string distance increases, the baryon vertex v also arises. The limiting case for the first state is when the baryon vertex v and the light quark q are heavy. The limiting case of the first configuration is that the position of the light quark reaches the vertex one. We can figure it out using the following formula:

$$g \frac{e^{sr_q^2}}{r_q} + ng \left(\frac{e^{\frac{1}{2}sr_q^2}}{r_q} \sqrt{f(r_q)} \right)' - \left(\frac{1}{3} A_0(r_q) \right)' = 0. \quad (37)$$

The first term is the string tension, the second is the force of the light quark, and the third is the force of the world sheet action.

Therefore, L and E can be calculated as

$$\begin{aligned} L &= 2 \int_0^{r_v} \partial_r x dr \\ &= 2 \int_0^{r_v} \sqrt{\frac{w^2(r_v) f^2(r_v)}{w^2(r) f^2(r) (f(r_v) + \tan^2 \alpha) - w^2(r_v) f^2(r_v) f(r)}}} dr, \end{aligned} \quad (38)$$

and

$$\begin{aligned} E &= 2g \int_0^{r_v} w(r) \sqrt{1 + f(r) \frac{w^2(r_v) f^2(r_v)}{w^2(r) f^2(r) (f(r_v) + \tan^2 \alpha) - w^2(r_v) f^2(r_v) f(r)}}} - \frac{1}{r^2} dr \\ &\quad - 2 \frac{g}{r_v} + g \int_{r_v}^{r_q} w(r) dr + 3gk \frac{e^{-2sr_v^2}}{r_v} \sqrt{f(r_v)} + ng \frac{e^{\frac{1}{2}sr_q^2}}{r_q} \sqrt{f(r_q)} - \frac{2}{3} A_0(0) - \frac{1}{3} A_0(r_q) + 2c. \end{aligned} \quad (39)$$

The plots for α , L , and E for the QQq small configuration are shown in Fig. 6.

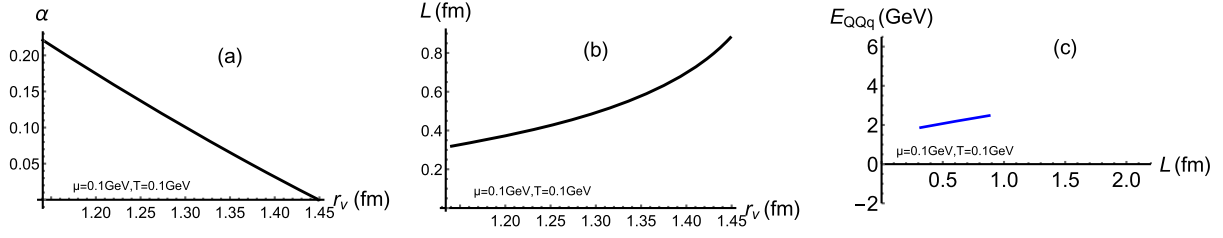


FIG. 7. (a) α as a function of r_v . (b) Separate distance L as a function of r_v . (c) The energy E as a function of L at $\mu = 0.1$ GeV, $T = 0.1$ GeV.

2. QQq intermediate

The total action in this configuration reads as

$$S = \sum_{i=1}^2 S_{\text{NG}}^{(i)} + S_{\text{vert}} + S_q + 2S_A|_{r=0} + S_A|_{r=r_q}, \quad (40)$$

that can be explicitly written as

$$S = \frac{2g}{T} \int dx \frac{e^{sr^2}}{r^2} \sqrt{f(r) + (\partial_x r)^2} + \frac{3kg}{T} \frac{e^{-2sr_v^2}}{r_v} \sqrt{f(r_v)} + \frac{ng}{T} \frac{e^{\frac{1}{2}sr_q^2}}{r_q} \sqrt{f(r_q)} - \frac{2A_0(0)}{3} \frac{1}{T} - \frac{1}{3} \frac{A_0(r_q)}{T}. \quad (41)$$

The force balance equation at the point $r = r_v$ is

$$\mathbf{e}_1 + \mathbf{e}_2 + \mathbf{f}_v + \mathbf{f}_q + \mathbf{f}_A = 0, \quad (42)$$

where each force is given by

$$\begin{aligned} \mathbf{f}_A &= (0, \partial_{r_q}(A_0(r_q))), \\ \mathbf{f}_q &= \left(0, -ng \partial_{r_q} \left(\frac{e^{\frac{1}{2}sr_q^2}}{r_q} \sqrt{f(r_q)} \right)\right), \\ \mathbf{f}_v &= \left(0, -3gk \partial_{r_v} \left(\frac{e^{-2sr_v^2}}{r_v} \sqrt{f(r_v)} \right)\right), \\ \mathbf{e}_1 &= gw(r_v) \left(-\frac{f(r_v)}{\sqrt{\tan^2 \alpha + f(r_v)}}, -\frac{1}{\sqrt{f(r_v)(\cot^2 \alpha + 1)}} \right), \\ \mathbf{e}_2 &= gw(r_v) \left(\frac{f(r_v)}{\sqrt{\tan^2 \alpha + f(r_v)}}, -\frac{1}{\sqrt{f(r_v)(\cot^2 \alpha + 1)}} \right), \end{aligned} \quad (43)$$

with $r_q = r_v$. The force balance equation leads to

$$2g \frac{e^{sr_v^2}}{r_v^2} \frac{1}{\sqrt{(1+f(r_v))\cot^2 \alpha}} + 3gk \partial_{r_v} \left(\frac{e^{-2sr_v^2}}{r_v} \sqrt{f(r_v)} \right) + ng \partial_{r_v} \left(\frac{e^{\frac{1}{2}sr_v^2}}{r_v} \sqrt{f(r_v)} \right) - \partial_{r_v}(A_v(r_v)) = 0. \quad (44)$$

The QQq becomes the second configuration, where the baryon vertices coincide with the light quarks. As the string distance increases, the baryon vertices and the light quarks move away from the heavy quarks. The angle α will tend to

zero in the second configuration. When α tends to be negative, the third state has to start. Now, the force equilibrium becomes

$$3gk \partial_{r_v} \left(\frac{e^{-2sr_v^2}}{r_v} \sqrt{f(r_v)} \right) + ng \partial_{r_v} \left(\frac{e^{\frac{1}{2}sr_v^2}}{r_v} \sqrt{f(r_v)} \right) - \partial_{r_v}(A_v(r_v)) = 0. \quad (45)$$

The solution to the equation is the limiting position of the second state.

Therefore, L and E can be calculated as

$$\begin{aligned} L &= 2 \int_0^{r_v} \partial_r x dr \\ &= 2 \int_0^{r_v} \sqrt{\frac{w^2(r_v) f^2(r_v)}{w^2(r)(f(r_v) + \tan^2 \alpha) f^2(r) - f(r) w^2(r_v) f^2(r_v)}}} dr \end{aligned} \quad (46)$$

and

$$\begin{aligned} E &= 2g \int_0^{r_v} w(r) \sqrt{1 + f(r)(\partial_r x)^2} - \frac{1}{r^2} dr - 2 \frac{g}{r_v} \\ &\quad + ng \frac{e^{\frac{1}{2}sr_v^2}}{r_v} \sqrt{f(r_v)} + 3gk \frac{e^{-2sr_v^2}}{r_v} \sqrt{f(r_v)} - \frac{2}{3} A_0(0) \\ &\quad - \frac{1}{3} A_0(r_q) + 2c. \end{aligned} \quad (47)$$

Plots for α , L , and E of QQq intermediate configuration are shown in Fig. 7.

3. QQq large

The total action for this configuration is the same as Eq. (40). Thus, the total action becomes

$$S = \frac{2g}{T} \int dx \frac{e^{sr^2}}{r^2} \sqrt{f(r) + (\partial_x r)^2} + \frac{ng}{T} \frac{e^{\frac{1}{2}sr_v^2}}{r_v} \sqrt{f(r_v)} + \frac{3g}{T} \frac{e^{-2sr_v^2}}{r_v} \sqrt{f(r_v)} - \frac{2A_0(0)}{3} \frac{1}{T} - \frac{1}{3} \frac{A_0(r_q)}{T}. \quad (48)$$

The Lagrangian density is written as

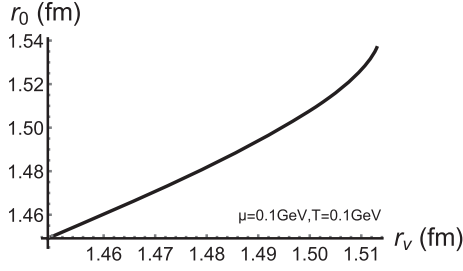


FIG. 8. r_0 as a function of r_v at $\mu = 0.1$ GeV and $T = 0.1$ GeV.

$$\mathcal{L} = \frac{e^{sr^2}}{r^2} \sqrt{f(r) + (\partial_x r)^2}, \quad (49)$$

with the constraint

$$\mathcal{L} - r' \frac{\partial \mathcal{L}}{\partial r'} = \frac{\frac{e^{sr^2}}{r^2} f(r)}{\sqrt{f(r) + (\partial_x r)^2}} = \text{constant}. \quad (50)$$

At the points r_0 and r_v , we have

$$\begin{aligned} \frac{\frac{e^{sr_0^2}}{r_0^2} f(r_0)}{\sqrt{f(r_0) + (\partial_x r)^2}} &= \frac{e^{sr_0^2}}{r_0^2} \sqrt{f(r_0)}, \\ \frac{\frac{e^{sr_v^2}}{r_v^2} f(r_v)}{\sqrt{f(r_v) + \tan^2 \alpha}} &= \frac{e^{sr_0^2}}{r_0^2} \sqrt{f(r_0)}. \end{aligned} \quad (51)$$

The above equations can determine the relation of r_0 , r_v , and α . We can also obtain

$$\partial_r x = \sqrt{\frac{\frac{e^{2sr_0^2}}{r_0^4} f^2(r_0)}{\frac{e^{2sr^2}}{r^4} f^2(r) f(r_0) - \frac{e^{2sr_0^2}}{r_0^4} f^2(r_0) f(r)}}} \quad (52)$$

and

$$\frac{e^{sr_v^2}}{r_v^2} f(r_v) - \frac{e^{sr_0^2}}{r_0^2} \sqrt{f(r_0)} \sqrt{f(r_v) + \tan^2 \alpha} = 0. \quad (53)$$

We can obtain the relationship between the highest point r_0 , the baryon vertex, and the position r_v of the light quark. The result is depicted in Fig. 8.

The force balance equation at the point $r_q = r_v$ is

$$\mathbf{e}_1 + \mathbf{e}_2 + \mathbf{f}_v + \mathbf{f}_q + \mathbf{f}_A = 0. \quad (54)$$

Each force is given by

$$\begin{aligned} \mathbf{f}_A &= (0, \partial_{r_q}(A_0(r_q))), \\ \mathbf{f}_q &= \left(0, -ng \partial_{r_q} \left(\frac{e^{\frac{1}{2}sr_q^2}}{r_q} \sqrt{f(r_q)} \right)\right), \\ \mathbf{f}_v &= \left(0, -3gk \partial_{r_v} \left(\frac{e^{-2sr_v^2}}{r_v} \sqrt{f(r_v)} \right)\right), \\ \mathbf{e}_1 &= gw(r_v) \left(-\frac{f(r_v)}{\sqrt{\tan^2 \alpha + f(r_v)}}, \frac{1}{\sqrt{f(r_v)(\cot^2 \alpha + 1)}} \right), \\ \mathbf{e}_2 &= gw(r_v) \left(\frac{f(r_v)}{\sqrt{\tan^2 \alpha + f(r_v)}}, \frac{1}{\sqrt{f(r_v)(\cot^2 \alpha + 1)}} \right). \end{aligned} \quad (55)$$

The force balance equation leads to

$$\begin{aligned} -2g \frac{e^{sr_v^2}}{r_v^2} \frac{1}{\sqrt{(1+f(r_v))\cot^2 \alpha}} + 3gk \partial_{r_v} \left(\frac{e^{-2sr_v^2}}{r_v} \sqrt{f(r_v)} \right) \\ + ng \partial_{r_v} \left(\frac{e^{\frac{1}{2}sr_v^2}}{r_v} \sqrt{f(r_v)} \right) - \partial_{r_v}(A_v(r_v)) = 0. \end{aligned} \quad (56)$$

Therefore, L and E can be calculated as

$$\begin{aligned} L &= 2 \left(\int_0^{r_0} \partial_r x dr + \int_{r_v}^{r_0} \partial_r x dr \right) \\ &= 2 \int_0^{r_0} \sqrt{\frac{\frac{e^{2sr_0^2}}{r_0^4} f^2(r_0)}{\frac{e^{2sr^2}}{r^4} f^2(r) f(r_0) - \frac{e^{2sr_0^2}}{r_0^4} f^2(r_0) f(r)}}} dr \\ &\quad + 2 \int_{r_v}^{r_0} \sqrt{\frac{\frac{e^{2sr_0^2}}{r_0^4} f^2(r_0)}{\frac{e^{2sr^2}}{r^4} f^2(r) f(r_0) - \frac{e^{2sr_0^2}}{r_0^4} f^2(r_0) f(r)}}} dr, \end{aligned} \quad (57)$$

$$\begin{aligned} E &= 2g \left(\int_0^{r_0} w(r) \sqrt{1+f(r)} \partial_r^2 x - \frac{1}{r^2} dr - \frac{1}{r_0} \right. \\ &\quad \left. + \int_{r_v}^{r_0} w(r) \sqrt{1+f(r)} \partial_r^2 x dr \right) + ng \frac{e^{\frac{1}{2}sr_v^2}}{r_v} \sqrt{f(r_v)} \\ &\quad + 3gk \frac{e^{-2sr_v^2}}{r_v} \sqrt{f(r_v)} - \frac{1}{3} A_0(r_q) - \frac{2}{3} A_0(0) + 2c. \end{aligned} \quad (58)$$

Plot for α , L , and E for the QQq large are shown in Fig. 9. Finally, we get the potential energy of QQq in Fig. 10.

C. $Q\bar{q}$, Qqq , qqq models

Now, let us examine the potential energy of the other three models. To do this, we must determine the positions of the light quarks q and \bar{q} . We can achieve this by utilizing the following three force equilibrium equations. The different configurations are shown in Fig. 11. For deeper explanations, see [43–45] whose conventions we generally follow.

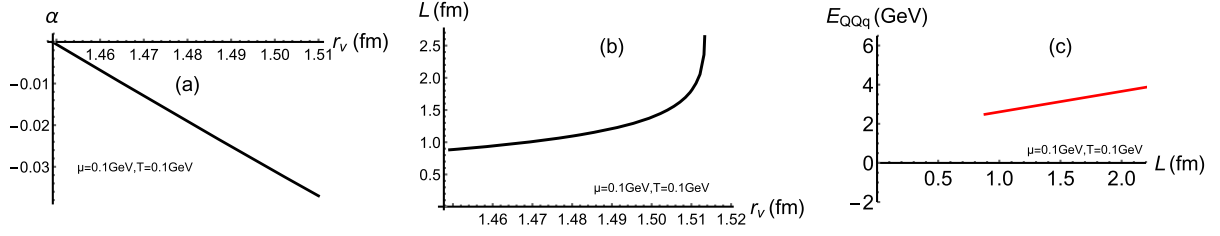


FIG. 9. Panel (a) α as a function of r_v . Panel (b) separation distance L as a function of r_v . Panel (c) the energy E as a function of L at $\mu = 0.1$ GeV, $T = 0.1$ GeV.

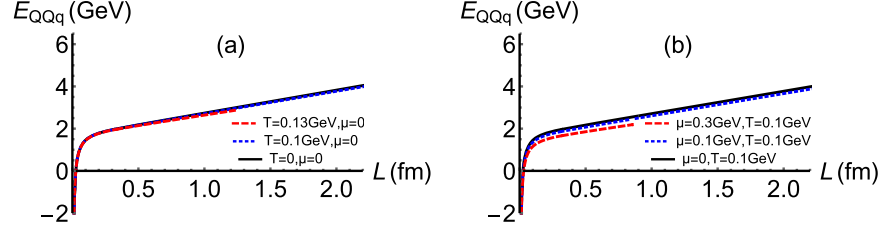


FIG. 10. QQq model: (a) The potential energy diagram for different temperatures at a chemical potential $\mu = 0$. (b) The potential energy diagram for different chemical potentials at a temperature of $T = 0.1$ GeV.

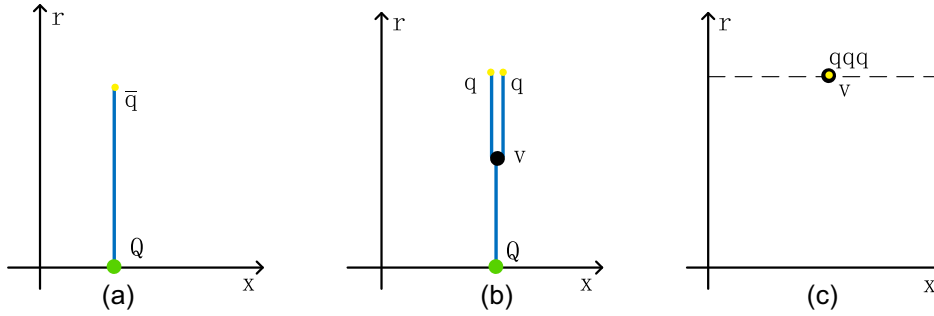


FIG. 11. Panel (a) is the configuration of $Q\bar{q}$. Panel (b) is the configuration of Qqq . Panel (c) is the configuration of qqq . Here $s = 0.450$ GeV, $g = 0.176$, $k = -\frac{1}{4}e^{\frac{1}{2}}$, and $c = 0.623$ GeV.

In $Q\bar{q}$ models, we get the force balance equation is

$$g \frac{e^{sr_{\bar{q}}}}{r_{\bar{q}}} + ng \left(\frac{e^{\frac{1}{2}sr_{\bar{q}}^2}}{r_{\bar{q}}} \sqrt{f(r_{\bar{q}})} \right)' + \left(\frac{1}{3}A_0(r_{\bar{q}}) \right)' = 0 \quad (59)$$

and the we can get the $r_{\bar{q}}$.

Then, in the Qqq models, we get the force balance equation r_v and r_q

$$g \frac{e^{sr_v^2}}{r_v^2} - 3gk \left(\frac{e^{-2sr_v^2}}{r_v} \sqrt{f(r_v)} \right)' = 0 \quad (60)$$

and

$$g \frac{e^{sr_q^2}}{r_q} + ng \left(\frac{e^{\frac{1}{2}sr_q^2}}{r_q} \sqrt{f(r_q)} \right)' - \left(\frac{1}{3}A_0(r_q) \right)' = 0. \quad (61)$$

Finally, in qqq models, r_q force balance is

$$3gk \left(\frac{e^{-2sr_q^2}}{r_q} \sqrt{f(r_q)} \right)' + 3ng \left(\frac{e^{\frac{1}{2}sr_q^2}}{r_q} \sqrt{f(r_q)} \right)' - (A_0(r_q))' = 0. \quad (62)$$

The potential energy of $Q\bar{q}$, Qqq , and qqq are

$$E_{Q\bar{q}} = g \int_0^{r_{\bar{q}}} \frac{e^{sr^2}}{r^2} - \frac{1}{r^2} dr - \frac{g}{r_{\bar{q}}} + ng \frac{e^{\frac{1}{2}sr_{\bar{q}}^2}}{r_{\bar{q}}} + \frac{1}{3}A_0(0) - \frac{1}{3}A_0(r_{\bar{q}}) + c, \quad (63)$$

$$\begin{aligned}
E_{Qqq} = & \mathfrak{g} \int_0^{r_v} \frac{e^{sr^2}}{r^2} - \frac{1}{r^2} dr - \frac{\mathfrak{g}}{r_v} + 2\mathfrak{g} \int_{r_v}^{r_q} \frac{e^{sr^2}}{r^2} dr \\
& + 2\mathfrak{ng} \frac{e^{\frac{1}{2}sr_q^2}}{r_q} + 3\mathfrak{gk} \frac{e^{-2sr_v^2}}{r_v} - \frac{2}{3}A_0(r_q) - \frac{1}{3}A_0(0) + c,
\end{aligned} \quad (64)$$

$$E_{qqq} = 3\mathfrak{gk} \frac{e^{-2sr_q^2}}{r_q} + 3\mathfrak{ng} \frac{e^{\frac{1}{2}sr_q^2}}{r_q} - A_0(r_q). \quad (65)$$

Therefore, we can compute the potential energy in case 3 and case 4. These energies can be calculated as

$$\begin{aligned}
E_{Qqq} + 2E_{Q\bar{q}} = & \mathfrak{g} \int_0^{r_v} \frac{e^{sr^2}}{r^2} - \frac{1}{r^2} dr - \frac{\mathfrak{g}}{r_v} + 2\mathfrak{g} \int_{r_v}^{r_q} \frac{e^{sr^2}}{r^2} dr \\
& + 2\mathfrak{ng} \frac{e^{\frac{1}{2}sr_q^2}}{r_q} + 3\mathfrak{gk} \frac{e^{-2sr_v^2}}{r_v} - \frac{2}{3}A_0(r_q) \\
& - \frac{1}{3}A_0(0) + 2\mathfrak{g} \int_0^{r_{\bar{q}}} \frac{e^{sr^2}}{r^2} - \frac{1}{r^2} dr \\
& - 2\frac{\mathfrak{g}}{r_{\bar{q}}} + 2\mathfrak{ng} \frac{e^{\frac{1}{2}sr_{\bar{q}}^2}}{r_{\bar{q}}} + \frac{2}{3}A_0(r_{\bar{q}}) \\
& - \frac{2}{3}A_0(0) + 3c,
\end{aligned} \quad (66)$$

$$\begin{aligned}
E_{qqq} + 3E_{Q\bar{q}} = & 3\mathfrak{gk} \frac{e^{-2sr_q^2}}{r_q} + 3\mathfrak{ng} \frac{e^{\frac{1}{2}sr_q^2}}{r_q} - A_0(r_q) \\
& + 3\mathfrak{g} \int_0^{r_{\bar{q}}} \frac{e^{sr^2}}{r^2} - \frac{1}{r^2} dr - 3\frac{\mathfrak{g}}{r_{\bar{q}}} \\
& + 3\mathfrak{ng} \frac{e^{\frac{1}{2}sr_{\bar{q}}^2}}{r_{\bar{q}}} + A_0(0) - A_0(r_{\bar{q}}) + 3c.
\end{aligned} \quad (67)$$

III. NUMERICAL RESULTS

We calculated the potential energy diagram for the ground state of triply heavy baryons, as shown in Fig. 12. This ground-state potential energy diagram is obtained under the conditions $T = 0$ and $\mu = 0$.

After analyzing the three-quark ground state, we calculated the potential energy diagrams for the finite temperature and finite chemical potential case. These diagrams are depicted in Fig. 13.

With these results, we can focus our study on two geometric configurations of the triply heavy quark system: $QQQ(A)$ with an equilateral triangular geometry and $QQQ(B)$ with a symmetric collinear geometry. The following contents will discuss the distinct patterns of string-breaking distances exhibited under these two configurations separately as the thermodynamic conditions are modulated.

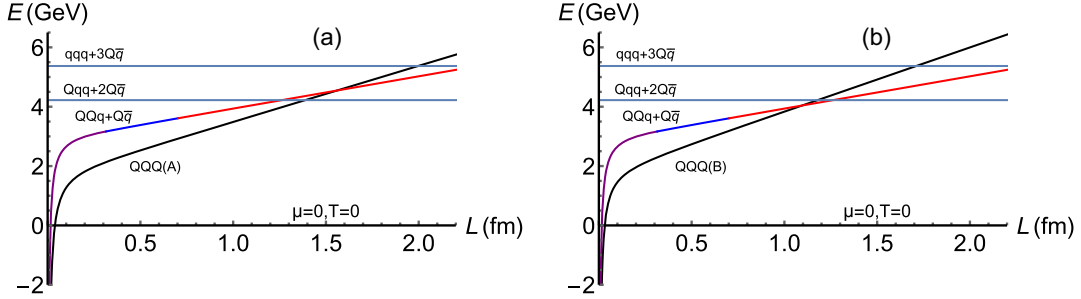


FIG. 12. Under the conditions $T = 0$ and $\mu = 0$, we plot the potential energy graphs of the quark states in four cases as a function of the distance between quarks. Panel (a) corresponds to the equilateral triangle geometry, and panel (b) corresponds to the symmetric collinear geometry.

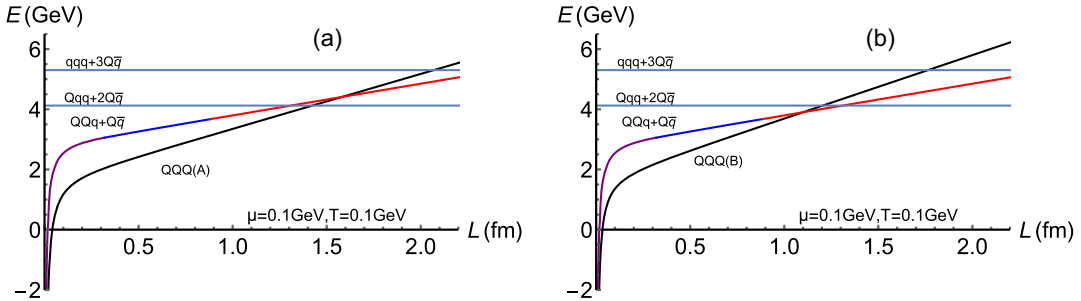


FIG. 13. By varying the temperature and chemical potential, we can analyze the impact of each one separately to obtain the fragmentation distance. In this context, panel (a) corresponds to the equilateral triangle geometry, and (b) corresponds to the symmetric collinear geometry.

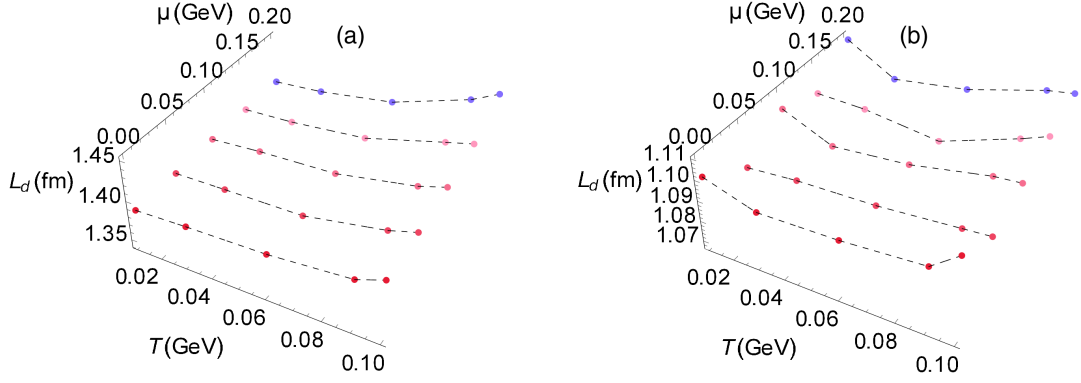


FIG. 14. Effect of temperature/chemical potential on the string-breaking distance. Panel (a) equilateral triangular geometry. Panel (b) symmetric collinear geometry.

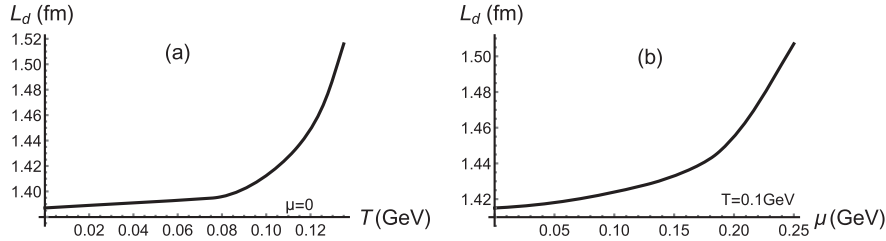


FIG. 15. The string-breaking distance of the $QQQ(A)$ configuration as a function of temperature and chemical potential is shown in the graph. Panel (a) represents the string-breaking distance at different temperatures when the chemical potential $\mu = 0$. Panel (b) represents the string-breaking distance at different chemical potentials when the temperature $T = 0.1$ GeV.

Based on the potential energy functions of inter-quark distances presented in Figs. 12 and 13, we have concluded that for the $QQQ(A)$ configuration with equilateral triangular geometry, the most likely decay mode is into $Qq\bar{q}$ and $2Q\bar{q}$, while for the $QQQ(B)$ configuration with symmetric collinear geometry, the most likely decay mode is into $QQ\bar{q}$ and $Q\bar{q}$.

We plotted the 3D landscapes showing the string-breaking distances for $QQQ(A)$ and $QQQ(B)$ varying with temperature and chemical potential.

The 3D relationships are depicted in Fig. 14. From the 3D landscapes, we extracted 2D distance-temperature and distance-chemical potential plots, as presented in Figs. 15 and 16, to investigate the effect of each thermodynamic factor individually.

It can be observed from the 2D plots that the effect of temperature and chemical potential on the string-breaking distance is more homogeneous in the equilateral triangular geometry while more complex in the symmetric collinear geometry. This phenomenon indicates the significant role of geometric configurations in determining the response of string-breaking distances to thermodynamic variations, which provides valuable insights.

For $QQQ(A)$ equilateral triangular geometry, the string-breaking distance exhibited a monotonic increasing trend as the temperature and chemical potential arose. This behavior indicates that the unique triangular configuration contributes to the consistent increment of string-breaking distance.

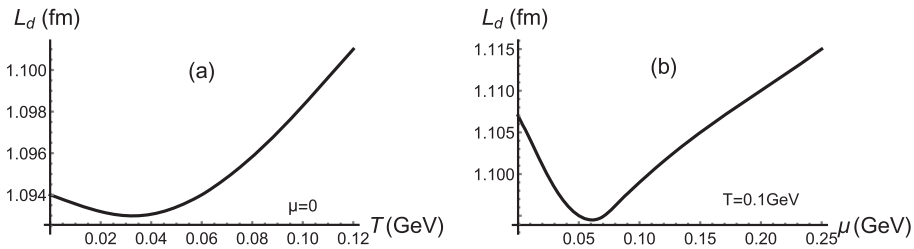


FIG. 16. The string-breaking distance of the $QQQ(B)$ configuration as a function of temperature and chemical potential is shown in the graph. Panel (a) represents the string-breaking distance at different temperatures when the chemical potential $\mu = 0$. Panel (b) represents the string-breaking distance at different chemical potentials when the temperature $T = 0.1$ GeV.

In contrast, for $QQQ(B)$ symmetric dyadic geometry, the string-breaking distance exhibits a nonmonotonic trend, decreasing and then sharply increasing before exceeding a threshold. This nonlinear behavior implies a complex transformation of the mechanical equilibrium conditions associated with the dyadic configuration. The underlying mechanisms need to be further investigated.

Importantly, chemical potential has a more pronounced effect on changing the string-breaking distances than temperature. This underscores the vital role of chemical potential in the dynamics and hadronization of triply heavy quarks.

IV. SUMMARY AND CONCLUSION

The deformed AdS-RN background model discussed in this work effectively explores the string-breaking processes of triply heavy quarks. We systematically investigated the dependence of string-breaking distances on two geometric configurations of triply heavy quarks (equilateral triangular

and symmetric collinear), finding that the differences in configurations significantly impact the trends in distance changes. We discovered that chemical potential has a more pronounced influence on changes in string-breaking distances compared to temperature. This study provides valuable new insights into the string-breaking distances of triply heavy quarks under varied temperature and chemical potential conditions.

ACKNOWLEDGMENTS

This work is supported by the Research Foundation of Education Bureau of Hunan Province, China (Grants No. 21B0402 and No. 20C1594) and the Natural Science Foundation of Hunan Province of China under Grants No. 2022JJ40344, the Key Laboratory of Quark and Lepton Physics Contract No. QLPL2022P01, and National Natural Science Foundation of China (NSFC) under the Grant No. 12205141 (J. Q.), No. 12350410371 (M. A. M. C.).

-
- [1] X. Artru, *Nucl. Phys.* **B85**, 442 (1975).
 - [2] G. C. Rossi and G. Veneziano, *Nucl. Phys.* **B123**, 507 (1977).
 - [3] N. Isgur and J. E. Paton, *Phys. Rev. D* **31**, 2910 (1985).
 - [4] G. Rossi and G. Veneziano, *J. High Energy Phys.* **06** (2016) 041.
 - [5] J. M. Maldacena, *Phys. Rev. Lett.* **80**, 4859 (1998).
 - [6] J. M. Maldacena, *Adv. Theor. Math. Phys.* **2**, 231 (1998).
 - [7] S. S. Gubser, I. R. Klebanov, and A. M. Polyakov, *Phys. Lett. B* **428**, 105 (1998).
 - [8] E. Witten, *Adv. Theor. Math. Phys.* **2**, 253 (1998).
 - [9] O. Andreev, *Phys. Rev. D* **93**, 105014 (2016).
 - [10] O. Andreev, *Phys. Lett. B* **756**, 6 (2016).
 - [11] O. Andreev, *Phys. Lett. B* **804**, 135406 (2020).
 - [12] O. Andreev, *J. High Energy Phys.* **05** (2021) 173.
 - [13] O. Andreev, *Phys. Rev. D* **104**, 026005 (2021).
 - [14] O. Andreev, *Phys. Rev. D* **105**, 086025 (2022).
 - [15] O. Andreev, *Phys. Rev. D* **106**, 066002 (2022).
 - [16] J. J. Jiang, Y. Z. Xiao, J. Qin, X. Li, and X. Chen, *Chin. Phys. C* **47**, 013106 (2023).
 - [17] S. V. Kadam, I. Raychowdhury, and J. R. Stryker, *Phys. Rev. D* **107**, 094513 (2023).
 - [18] M. Baker, P. Cea, V. Chelnokov, L. Cosmai, F. Cuteri, and A. Papa, *Eur. Phys. J. C* **80**, 514 (2020).
 - [19] I. T. Drummond, *Phys. Lett. B* **434**, 92 (1998).
 - [20] J. Bulava, B. Hörz, F. Knechtli, V. Koch, G. Moir, C. Morningstar, and M. Peardon, *Phys. Lett. B* **793**, 493 (2019).
 - [21] G. S. Bali, *Phys. Rep.* **343**, 1 (2001).
 - [22] G. S. Bali, B. Bolder, N. Eicker, T. Lippert, B. Orth, P. Ueberholz, K. Schilling, and T. Struckmann (SESAM and $T\chi L$ Collaborations), *Phys. Rev. D* **62**, 054503 (2000).
 - [23] C. R. Allton *et al.* (UKQCD Collaboration), *Phys. Rev. D* **60**, 034507 (1999).
 - [24] C. Michael and P. Pennanen (UKQCD Collaboration), *Phys. Rev. D* **60**, 054012 (1999).
 - [25] P. Pennanen *et al.* (UKQCD Collaboration), arXiv:hep-lat/0001015.
 - [26] K. Schilling, *Nucl. Phys. B, Proc. Suppl.* **83**, 140 (2000).
 - [27] N. A. Campbell, I. H. Jorysz, and C. Michael, *Phys. Lett.* **167B**, 91 (1986).
 - [28] C. Szasz and M. Wagner, *Phys. Rev. D* **78**, 036006 (2008).
 - [29] C. Michael, *Nucl. Phys. B, Proc. Suppl.* **26**, 417 (1992).
 - [30] J. M. Flynn, E. Hernandez, and J. Nieves, *Phys. Rev. D* **85**, 014012 (2012).
 - [31] G. S. Bali, H. Neff, T. Düssel, T. Lippert, and K. Schilling (SESAM Collaboration), *Phys. Rev. D* **71**, 114513 (2005).
 - [32] D. Antonov, *Universe* **9**, 97 (2023).
 - [33] O. Andreev and V. I. Zakharov, *J. High Energy Phys.* **04** (2007) 100.
 - [34] C. P. Herzog, *Phys. Rev. Lett.* **98**, 091601 (2007).
 - [35] P. Colangelo, F. Giannuzzi, and S. Nicotri, *Phys. Rev. D* **83**, 035015 (2011).
 - [36] Z. q. Zhang, D. f. Hou, and G. Chen, *Nucl. Phys.* **A960**, 1 (2017).
 - [37] X. Chen, B. Yu, P. C. Chu, and X. h. Li, *Chin. Phys. C* **46**, 073102 (2022).
 - [38] O. Andreev, *Phys. Rev. D* **101**, 106003 (2020).
 - [39] I. Bars and M. B. Green, *Phys. Rev. D* **17**, 537 (1978).
 - [40] C. Alexandrou, P. de Forcrand, and O. Jahn, *Nucl. Phys. B, Proc. Suppl.* **119**, 667 (2003).
 - [41] O. Andreev, *Phys. Rev. D* **73**, 107901 (2006).
 - [42] O. W. Greenberg and H. J. Lipkin, *Nucl. Phys.* **A370**, 349 (1981).
 - [43] O. Andreev, *Phys. Rev. D* **94**, 126003 (2016).
 - [44] O. Andreev, *Phys. Rev. Lett.* **102**, 212001 (2009).
 - [45] O. Andreev and V. I. Zakharov, *Phys. Lett. B* **645**, 437 (2007).